

Two-photon absorption in gapped bilayer graphene with a tunable chemical potential

M. K. Brinkley¹

D. S. L. Abergel^{2,3}

B. D. Clader¹

¹Johns Hopkins University Applied Physics Laboratory, Research and Exploratory Development Department, Laurel, MD 20973

²Nordita, KTH Royal Institute of Technology and Stockholm University, Roslagstullsbacken 23, SE-106 91 Stockholm, Sweden

³Center for Quantum Materials, KTH and Nordita, Roslagstullsbacken 11, SE-106 91 Stockholm, Sweden

Abstract. Despite the now vast body of two-dimensional materials under study, bilayer graphene remains unique in two ways: it hosts a simultaneously tunable band gap and electron density; and stems from simple fabrication methods. These two advantages underscore why bilayer graphene is critical as a material for optoelectronic applications. In the work that follows, we calculate the one- and two-photon absorption coefficients for degenerate interband absorption in a graphene bilayer hosting an asymmetry gap and adjustable chemical potential—all at finite temperature. Our analysis is comprehensive, characterizing one- and two-photon absorptive behavior over wide ranges of photon energy, gap, chemical potential, and thermal broadening. The two-photon absorption coefficient for bilayer graphene displays a rich structure as a function of photon energy and band gap due to the existence of multiple absorption pathways and the nontrivial dispersion of the low energy bands. This systematic work will prove integral to the design of bilayer-graphene-based nonlinear optical devices.

The excitement following the isolation of graphene [1] is due in part to the remarkable optoelectronic properties the material possesses [2, 3]. In addition to a high electron mobility [4] and fast optical response [5], graphene and its bilayer (BLG) exhibit tunable broadband optical absorption [3, 6, 7, 9, 8], suggesting applicability to such devices as optical modulators [9, 10], photodetectors [11, 12], and possibly all-optical switches [13, 14, 15, 16]. Recent studies have revealed that graphene has a large third-order susceptibility [17, 18], leading to a strong two-photon absorption (2PA) coefficient [19], which is stronger yet in the bilayer system [20] due to the nested manifold of bands present at the K -point of the Brillouin zone. As a result of this K -point band-commensuration and the larger number of absorptive pathways, the 2PA coefficient for the ungapped bilayer system is several orders of magnitude higher than that of monolayer graphene (MLG) in certain frequency ranges [20].

Despite the attractive optoelectronic properties of undoped and gapless graphene systems, the absence of a gap at the K -point precludes MLG from use in many device applications. Multilayer graphene systems, however, do exhibit a band gap when chemically doped or externally gated, permitting a wide range of control over the conductivity. In fact, by simultaneous use of top and bottom gating, the carrier density and gap size can be independently tuned [21], providing a degree of dynamical control of the optical response not available in many optoelectronic materials. Below, we demonstrate that the 2PA of bilayer graphene displays a rich structure as a function of these two parameters.

Moreover, as the doping concentration of graphene is very sensitive [22] to synthesis methodology and conditions, a characterization of doped, gapped graphene systems will prove paramount to experimental characterization and successful device design.

At present, a theoretical characterization of the 2PA strength in doped, gapped BLG has yet to be reported, and calculations of the 2PA coefficient [20] in the ungapped system are incomplete since they do not encompass all possible intermediate states. Here, we compute using a perturbative approach the full one- and two-photon absorption coefficients for a graphene bilayer with a band gap and a tunable chemical potential. The physical scenario we discuss is a back-gated graphene bilayer placed underneath a transparent top gate (see, for example, Ref. [23]), providing simultaneous and independent control over the chemical potential, μ , and the asymmetry gap, Δ . The one-photon absorption (1PA) spectrum for the gapped system has been computed previously by Nicol and Carbotte [24], which we reproduce for comparison to the 2PA spectrum.

An electric field oriented perpendicular to a Bernal-stacked graphene bilayer gives rise to an asymmetry gap [25], for which the tight-binding Hamiltonian in the K -valley using the basis (A1,B2,A2,B1) in the sublattice space is

$$\hat{\mathcal{H}}_{TB} = \begin{bmatrix} -\Delta/2 & 0 & 0 & \gamma_1 \rho e^{-i\phi} \\ 0 & \Delta/2 & \gamma_1 \rho e^{i\phi} & 0 \\ 0 & \gamma_1 \rho e^{-i\phi} & \Delta/2 & \gamma_1 \\ \gamma_1 \rho e^{i\phi} & 0 & \gamma_1 & -\Delta/2 \end{bmatrix}. \quad (1)$$

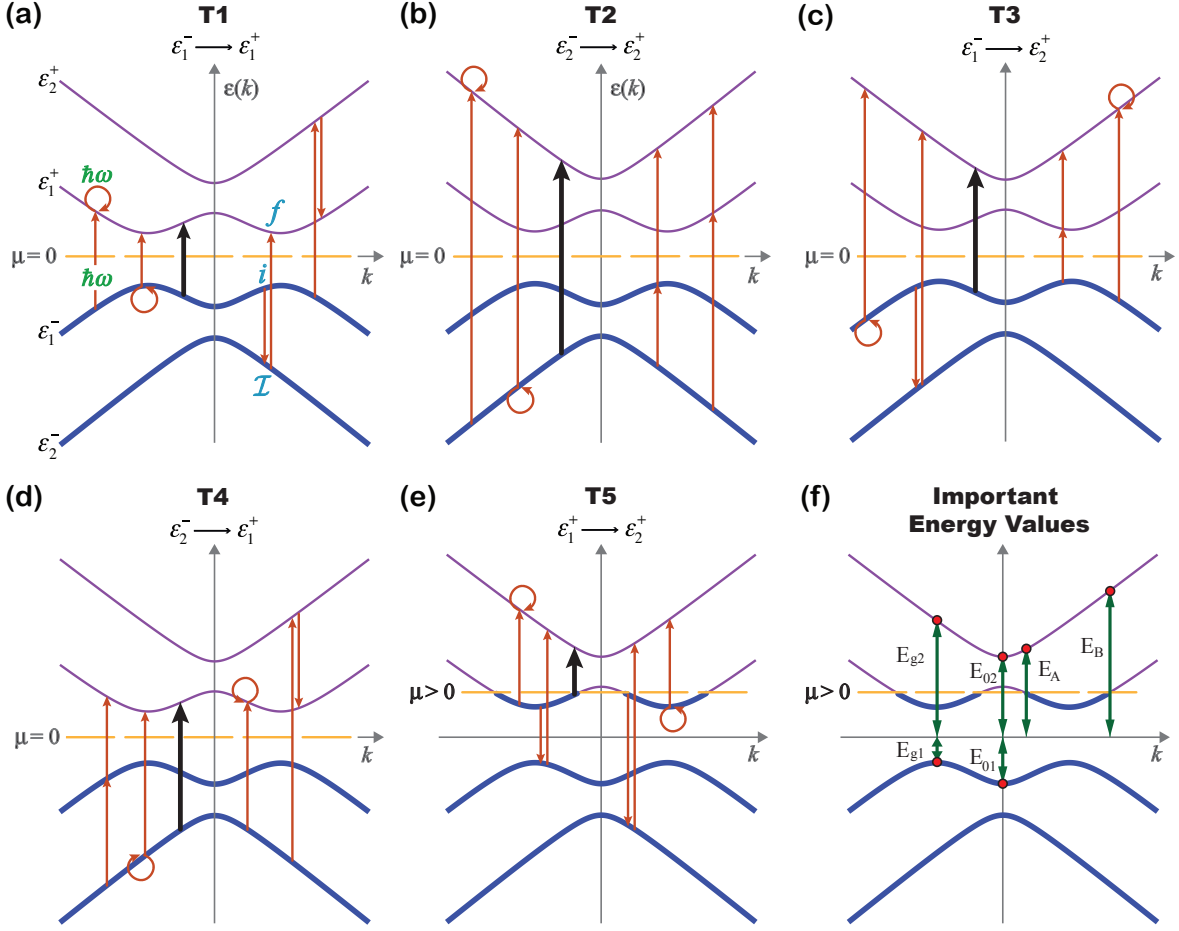


Figure 1. (a)-(e) Illustrations of the allowed 1PA (thick black arrows) and 2PA (thin red arrows) transitions, $T1 - T5$, in a gapped graphene bilayer at $T = 0$. The thick dashed line represents the chemical potential, and the thick (thin) curves denote populated (unpopulated) bands. The circular arrows signify transitions for which $|i\rangle \rightarrow |\mathcal{I} = i\rangle$ or $|\mathcal{I}\rangle \rightarrow |f = \mathcal{I}\rangle$. (f) Important energy values for the gapped band structure are indicated with green arrows, as defined in Ref. [24].

We use the following notation: $\phi = \tan^{-1}(p_y/p_x)$ is the polar angle of the in-plane momentum, \mathbf{p} ; $\rho \equiv v_F p / \gamma_1$ is the reduced momentum; $\gamma_1 = 0.4$ eV is the A2-B1 interlayer coupling; and $v_F \sim 10^6 \text{ms}^{-1}$ is the Fermi velocity. The corresponding exact eigenvalues and eigenvectors are

$$\varepsilon_j^\pm = \pm \left(\gamma_1^2 \rho^2 + \frac{\Delta^2}{4} + \frac{\gamma_1^2}{2} + \gamma_1 (-1)^j \sqrt{\rho^2 (\Delta^2 + \gamma_1^2) + \frac{\gamma_1^2}{4}} \right)^{1/2} \quad (2)$$

and

$$|\psi_j^\pm(\rho)\rangle = \frac{1}{\mathcal{N}_j} \begin{bmatrix} \frac{2\gamma_1 \rho \exp(-i\phi)}{2\varepsilon_j^\pm + \Delta} \\ \frac{2\gamma_1^2 \rho \exp(i\phi)}{c_j - 2\varepsilon_j^\pm \Delta} \\ \frac{\gamma_1 (2\varepsilon_j^\pm - \Delta)}{c_j - 2\varepsilon_j^\pm \Delta} \\ 1 \end{bmatrix} \quad (3)$$

where $j = 1(2)$ denotes the low-energy (high-energy) bands split by Δ at the K -point; \mathcal{N}_j is a normalization factor; and $\mathcal{C}_j \equiv \Delta^2 + \gamma_1^2 + (-1)^j \sqrt{4\Delta^2\rho^2 + 4\gamma_1^2\rho^2 + \gamma_1^2}$. For an incident field with polarization chosen along the x direction, $\mathbf{A}(t) = A_0\hat{x}\exp(i\omega t)$, the interaction Hamiltonian is

$$\hat{\mathcal{H}}_{int} = \frac{e}{2mc}\mathbf{A} \cdot \hat{\mathbf{p}} = \frac{e}{2c}\left|\frac{ic}{\omega}\mathbf{E}\right|\hat{x} \cdot \hat{\mathbf{v}} = \frac{e}{2\omega}E_0\frac{\partial\hat{\mathcal{H}}_{TB}}{\partial p_x}. \quad (4)$$

Assuming a relative permittivity $\epsilon_r \approx 9$ for BLG [26, 27] and an incident irradiance $I = E_0^2 c \epsilon_0 \sqrt{\epsilon_r}/2$, perturbation theory gives the one- and two-photon absorption coefficients [28, 29], which are, respectively,

$$\beta_1 = \frac{2\hbar\omega}{I} \frac{2\pi}{\hbar} g \sum_{i,f} \left| \langle f | \hat{\mathcal{H}}_{int} | i \rangle \right|^2 \delta(\epsilon_f - \epsilon_i - \hbar\omega) \quad (5)$$

and

$$\beta_2 = \frac{4\hbar\omega}{I^2} \frac{2\pi}{\hbar} g \sum_{i,f} \left| \sum_{\mathcal{I}} \frac{\langle f | \hat{\mathcal{H}}_{int} | \mathcal{I} \rangle \langle \mathcal{I} | \hat{\mathcal{H}}_{int} | i \rangle}{\epsilon_{\mathcal{I}} - \epsilon_i - \hbar\omega} \right|^2 \delta(\epsilon_f - \epsilon_i - 2\hbar\omega), \quad (6)$$

where $\beta_n \equiv 2n\hbar\omega W_n/I^n$ is the n -photon absorption coefficient; W_n represents the n^{th} -order interband transition probability rate per unit area; $g = 4$ is a factor accounting for spin and valley degeneracy; and the subscripts label the initial (i), intermediate (\mathcal{I}) and final (f) states.

Figure 1 shows the band structure at the K -point for a gapped graphene bilayer. The interband 1PA and 2PA transitions are shown, each of which must satisfy the constraints of energy and momentum conservation imposed by the δ -functions in the expressions for β_n . For the case of 1PA, the thick black arrows in Fig. 1(a)-(d) denote the four one-photon pathways (T1-T4) permitted from $\epsilon_i \rightarrow \epsilon_f$ for a neutral chemical potential ($\mu = 0$) at a temperature of $T = 0$ K. The thick arrow in the fifth panel, Fig. 1(e), illustrates T5, the transition allowed from $\epsilon_1^+ \rightarrow \epsilon_2^+$ when $\mu > 0$.

Associated with each 1PA transition is a family of possible 2PA pathways [30], which are illustrated in Fig. 1 by thin red arrows. In the case of 2PA, two photons are absorbed simultaneously via two energy-nonconserving transitions of $|i\rangle \rightarrow |\mathcal{I}\rangle$ and $|\mathcal{I}\rangle \rightarrow |f\rangle$, for which energy is conserved over $|i\rangle \rightarrow |f\rangle$. For each of the initial and final state combinations, four pathways are possible, all of which are indicated in Fig. 1. The transitions T3 and T4 displayed in Fig. 1(c) and (d) are degenerate. A determination of the criteria imposed on T1-T5 by energy conservation requires the calculation of several important energy values, which are provided for reference in Fig. 1(f) using the nomenclature of Nicol and Carbotte [24] and we shall refer to these values below. We confine our analysis to the case $\mu \geq 0$ since electron-hole symmetry implies that the response is identical for $\mu < 0$.

The diagrams in Fig. 1 and the denominator of Eq. (6) allow for several immediate insights into the frequency response of β_2 when $\Delta = 0$ and $T = 0$. The transitions taking part in the 2PA process for which $|i\rangle \rightarrow |\mathcal{I} = i\rangle$ or $|\mathcal{I}\rangle \rightarrow |f = \mathcal{I}\rangle$, denoted by circular arrows, produce a singularity in β_2 at $\hbar\omega = 0$. When Δ becomes large compared to the

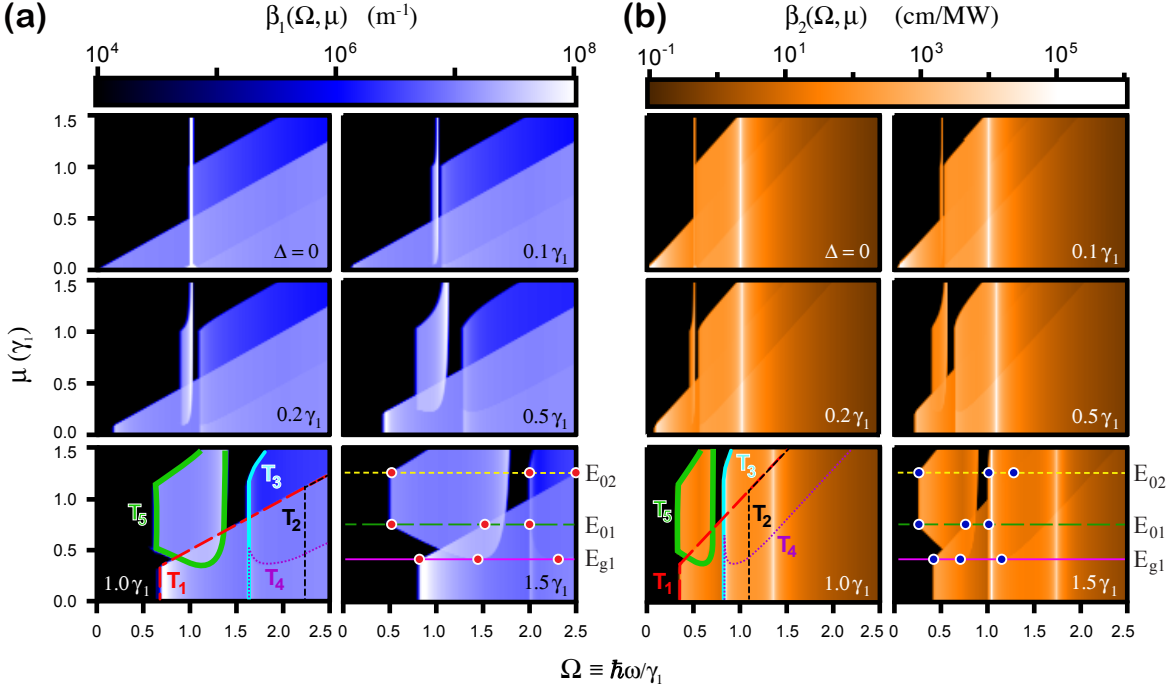


Figure 2. Color plots of the (a) one-photon absorption coefficient, $\beta_1(\Omega, \mu)$, and (b) two-photon absorption coefficient, $\beta_2(\Omega, \mu)$, for a wide range of the gap, Δ , and chemical potential, μ . The color scale at the top of each panel indicates the intensity of β_1 and β_2 . The (μ, Ω) regions of spectral weight associated with each transition, T1-T5, are delineated in both (a) and (b) for $\Delta = \gamma_1$, showing how each transition (labeled in Fig. 1) contributes to the 1PA or 2PA coefficient. The panels for $\Delta = 1.5\gamma_1$ depict the relevant energy thresholds illustrated in Fig. 1(f). The colored circles mark the changes in spectral weight that result as μ crosses E_{g1} , E_{01} , and E_{02} .

temperature, this resonance disappears since there are no pairs of initial and final states which satisfy the δ -function. Similarly, contributions for which $\varepsilon_f - \varepsilon_i = 2\hbar\omega = 2\gamma_1$ produce a singularity at γ_1 , and 2PA transitions for which $\varepsilon_f - \varepsilon_i = 2\hbar\omega = \gamma_1$ give rise to a singularity at $\hbar\omega = \gamma_1/2$. For 1PA when $\mu \geq 0$ and $T > 0$, a singularity exists only due to T5, which generates an intense, narrow peak at $\hbar\omega = \gamma_1$ when bands ε_1^+ and ε_2^+ are perfectly nested. This peak will exist for $T > 0$ even when $\mu = 0$ due to thermal population of conduction band $\varepsilon_1^+(\rho)$ and depopulation of valence band $\varepsilon_1^-(\rho)$.

When an asymmetry gap $\Delta > 0$ is present, the conditions imposed by energy conservation become more complex [24] due to the so-called “sombbrero” structure [25] of the low-energy bands ε_1^\pm . The bands are not perfectly nested as they are for $\Delta = 0$, leading to the rich absorptive structure displayed in Fig. 2. Figure 2 shows color plots of both the 1PA and 2PA coefficients for a wide range of gap values. Note that the highest value of $\Delta = 1.5$ is probably unattainable using current experimental techniques, but we wish to display the effects when $\Delta \geq 1$ since several spectral features change. A transformation of $\omega \rightarrow \omega + i\Gamma/\hbar$ accounts for thermal broadening and we take $\Gamma = 5.4 \times 10^{-3}\gamma_1$, which corresponds to a temperature of $T = 25$ K.

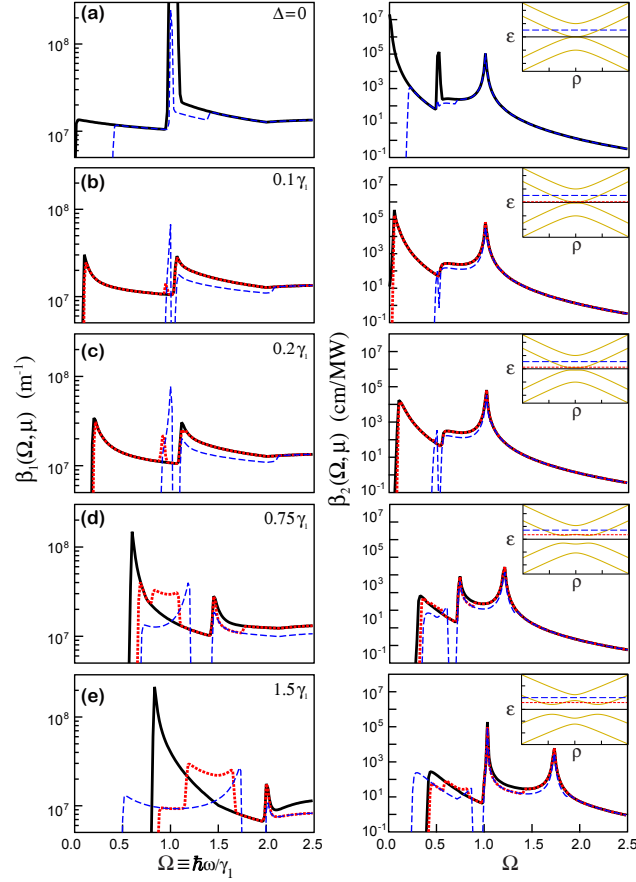


Figure 3. 1PA (left column) and 2PA (right column) for the indicated value of the gap, Δ . The solid, dotted, and dashed curves correspond to the identical lines superimposed on the dispersion curves in the insets in the right-hand column, indicating the absorption for chemical potentials of $\mu = 0$ (continuous black line), $\mu = (E_{g1} + E_{01})/2$ (dotted red line), and $\mu = (E_{01} + E_{02})/2$ (dashed blue line).

The thermal broadening leads to the emergence in Fig. 2(a) of an intense, narrow peak at $\hbar\omega = \gamma_1$ due to T5 for $\Delta = 0$ (see Ref. [31]). At $T = 25$ K, band ε_1^+ receives spectral weight due to thermal population, giving rise to T5 transitions of $\varepsilon_1^+ \rightarrow \varepsilon_2^+$. Similarly, in the β_2 spectrum for $\Delta = 0$ in Fig. 1(b), the thermal smearing of μ leads to a peak at $\hbar\omega = \gamma_1/2$, as anticipated during the analysis of Fig. 1. When Δ is small, the $1/\Omega$ divergence in the 2PA is caused by the resonance near the center of the Brillouin zone. This is not present in the 1PA because it is cancelled by the absorption matrix element. When Δ increases, the T5 component of both β_1 and β_2 broadens into the cleaver-shaped regions outlined in green for $\Delta = \gamma_1$ in Fig. 2(a,b). The asymmetric broadening of the T5 region is due to the sombrero shape of ε_1^\pm and the loss of spectral weight when $\mu > E_{02}$. The panels corresponding to $\Delta = \gamma_1$ in Fig. 2(a) and (b) identify the energy thresholds mapped in Fig. 1(f), illustrating regions where the chemical potential either blocks or permits absorptive pathways. For $\Delta > 0$, the band gap means that there is no absorption at $\Omega < 2E_{g1}$ and the increased density of states at the band edge produces

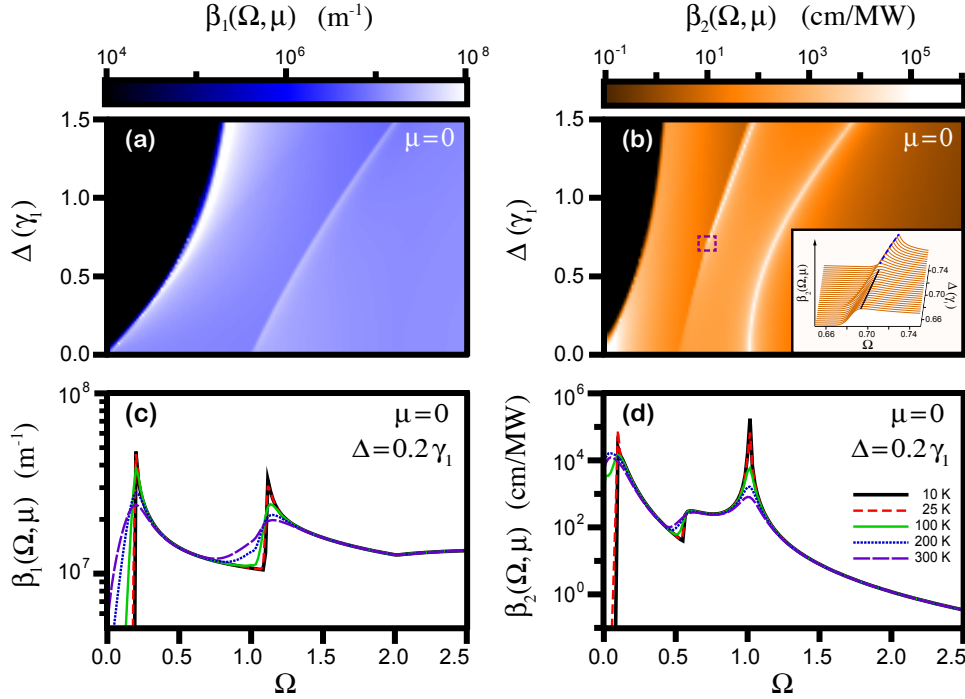


Figure 4. Spectra of the (a) one-photon absorption coefficient, $\beta_1(\Omega, \Delta)$, and (b) two-photon absorption coefficient, $\beta_2(\Omega, \Delta)$, for which $\mu = 0$ and Γ corresponds to 25 K. The inset in (b) contains the region outlined by the dashed purple box, in which a dashed blue line traces an emerging peak and a black dotted line indicates the T3/T4 cutoff. Panels (c) and (d) display spectra of $\beta_1(\Omega, T)$ and $\beta_2(\Omega, T)$, respectively, for $\Delta = 0.2\gamma_1$ and $\mu = 0$.

regions of increasing 1PA and 2PA near the T1 cutoff. The other spectrally empty region that emerges with increasing Δ occurs between the T3/T4 and T5 pockets.

In contrast with the $\varepsilon_f - \varepsilon_i = \hbar\omega$ requirement of 1PA, 2PA requires $\varepsilon_f = \varepsilon_i = 2\hbar\omega$, which compresses and shifts the T1-T5 regions in β_2 relative to those β_1 . Also, Eq. (6) shows that the resonances will be stronger in the 2PA due to the additional factor of $(\hbar\omega - \varepsilon_{\mathcal{I}} + \varepsilon_i)^{-2}$ in the sum over intermediate states. The spectra for β_2 shown in Fig. 2(b) contain a prominent resonance not present in β_1 . This β_2 resonance, arising at $\Omega = 1$ when $\Delta = 0$, is due to transitions T3 and T4, which contain denominators of $\hbar\omega - \gamma_1$ and give rise to a singularity. As Δ increases, this resonance shifts toward higher Ω due to the increasing size of the band gap. At this T3/T4 resonance, the BLG 2PA strength is several orders of magnitude larger for bilayer graphene than for monolayer graphene [20].

Figure 3 presents 1PA and 2PA curves extracted from the color maps of Fig. 2, grouped by gap value. The left-hand column shows $\beta_1(\Omega, \mu)$, and the right-hand column shows $\beta_2(\Omega, \mu)$. For each plot of β_1 and β_2 , several values of μ are chosen, each of which corresponds to an identical horizontal line on the accompanying dispersion shown in the inset to the β_2 plots. The solid black curves are for $\mu = 0$; the dotted red is for $\mu = (E_{g1} + E_{01})/2$ which is where the chemical potential is in the middle of the sombrero

region; the dashed blue line is for $\mu = (E_{01} + E_{02})/2$, and lies halfway between ε_1^+ and ε_2^+ at $\rho = 0$. When $\Delta = 0$, the dotted red slice is equivalent to that of $\mu = 0$, so that the solid black and dotted red lines are identical. As $\Omega \rightarrow \infty$, the contributions to β_2 of transitions T1-T4 tend to $1/\Omega^4$.

Figure 3 reveals an intense, narrow peak in β_2 that emerges when $\Delta \geq \gamma_1/\sqrt{2}$, resulting from two $|i\rangle \rightarrow |\mathcal{I}\rangle$ routes within the family of T3 and T4 pathways. In particular, routes $\varepsilon_1^- \rightarrow \varepsilon_1^+$ and $\varepsilon_1^- \rightarrow \varepsilon_2^-$ lead to a vanishing denominator $\varepsilon_{\mathcal{I}} - \varepsilon_i - \hbar\omega$ in Eq. (6) at values of

$$\Omega_A \equiv \frac{\sqrt{2}}{4\gamma_1} \left(5(\Delta^2 + \gamma_1^2) - 3\sqrt{\Delta^4 + \frac{2}{9}\Delta^2\gamma_1^2 + \gamma_1^4} \right)^{1/2}. \quad (7)$$

When $\Omega = \Omega_A$ and $\Delta \geq \gamma_1/\sqrt{2}$ for $\Gamma = 0$, the position of the peak, Ω_A , eclipses the T3/T4 cutoff, causing the peak to appear when the photon energy $\hbar\omega = \Omega\gamma_1$ coincides with $\varepsilon_1^+ - \varepsilon_1^- \geq (E_{01} + E_{02})/2$ and $\varepsilon_1^- - \varepsilon_2^- \geq (E_{01} + E_{02})/2$.

Figure 4(a) and (b) show β_1 and β_2 as a function of Ω and Δ for $T = 25$ K and $\mu = 0$. As Δ increases from 0, certain regions of increasing intensity materialize in both 1PA and 2PA spectra, including the peak in β_2 at Ω_A , which is outlined in Fig. 4(b) by a dashed purple box surrounding the point $(\Omega, \Delta) = (1/\sqrt{2}, \gamma_1/\sqrt{2})$. The inset in Fig. 4(b) provides a zoomed-in view of the boxed region, in which the dotted black line indicates the T3/T4 cutoff, and the dashed blue line shows the onset of the emerging peak. Thus far, the assumed thermal broadening corresponds to a temperature of 25 K — a value large enough to reveal the T5 resonance when $\mu = 0$, yet small enough to avoid the smearing of fine features. Figure 4 (c) and (d) illustrate the effect of thermal broadening on β_1 and β_2 for $\Delta = 0.2\gamma_1$ at neutral doping ($\mu = 0$). The most pronounced impact of increasing temperature is the broadening of β_1 and β_2 into the gap region. Once Γ reaches room temperature, the otherwise abrupt T3/T4 cutoff just beyond $\Omega = 1$ spreads into a more diffuse spectral bulge. Similarly, the sharp β_2 resonance residing near $\Omega = 1$ at $T = 10$ K suffers appreciably within the temperature range examined, dropping in intensity by more than two orders of magnitude when $T = 300$ K.

We have demonstrated that when an electric field is applied perpendicular to a graphene bilayer, the resulting asymmetry gap gives rise to complex linear and nonlinear optical absorption. This is experimentally verifiable in a simple photoabsorption measurement using transparent gates. For the gapped bilayer system with a tunable chemical potential, we have calculated both one- and two-photon absorption spectra over an expansive range of the gap and chemical potential, taking into account all possible absorption pathways in the calculation of $\beta_2(\Omega, \mu)$. We analyze the 2PA resonances that emerge in the gapped, doped bilayer system, and examine the evolution of these resonances as a function of Δ and μ . The effects of thermal broadening are incorporated into the computations, providing insight into the degradation of optical performance at or near room temperature. As graphene-based optical architectures mature, the absorption spectra calculated above will prove important for optimizing and enhancing device performance.

Acknowledgments

This work was supported by Internal Research & Development funds and the Stuart S. Janney Fellowship Program at the Johns Hopkins University Applied Physics Laboratory. MKB thanks Tai-Chang Chiang, Yang Liu, Scott Hendrickson, and Joan Hoffmann for their valuable comments and insight. DLSA is supported by Nordita and by ERC project DM-321031.

References

- [1] D. S. L. Abergel, V. Apalkov, J. Berashevich, K. Ziegler, and T. Chakraborty, *Adv. Phys.* **59**, 261 (2010).
- [2] A. K. Geim, *Science* **324** 1530 (2009).
- [3] R. R. Nair, P. Blake, A. N. Grigorenko, K. S. Novoselov, T. J. Booth, T. Stauber, N. M. R. Peres, and A. K. Geim, *Science* **320**, 1308 (2008).
- [4] C. Berger, Z. Song, T. Li, X. Li, A. Y. Ogbazghi, R. Feng, Z. Dai, A. N. Marchenkov, E. H. Conrad, P. N. First, and W. A. de Heer, *J. Phys. Chem. B* **108**, 19912 (2004).
- [5] S.-F. Shi, T.-T. Tang, B. Zeng, L. Ju, Q. Zhou, A. Zettl, and F. Wang, *Nano Lett.* **14**, 1578 (2014).
- [6] D. S. L. Abergel and V. I. Fal'ko, *Physical Review B* **75**, 155430 (2007).
- [7] Hongki Min, D. S. L. Abergel, E. H. Hwang, and S. Das Sarma, *Physical Review B* **84**, 041406 (2011).
- [8] C.-H. Park and Louie, S. G., *Nano Lett.* **10**, 426 (2010).
- [9] M. Liu, X. Yin, E. Avila-Ulin, B. Geng, T. Zentgraf, L. Ju, F. Wang, and X. Zhang, *Nature* **474**, 64 (2011).
- [10] S. J. Koester and M Li, *Applied Physics Letters* **100**, 171107 (2012).
- [11] F. Xia, T. Mueller, Y. Lin, A. Valdes-Garcia, and P. Avouris, *Nature Nanotechnology* **4**, 839 (2009).
- [12] Z. Fang, Z. Liu, Y. Wang, P. M. Ajayan, P. Nordlander, and N. J. Halas, *Nano Letters* **12**, 3808 (2012).
- [13] T. Volz, A. Reinhard, M. Winger, A. Badolato, K. J. Hennessy, E. L. Hu, and A. Imamoglu, *Nature Photonics* **6**, 605 (2012).
- [14] S. M. Hendrickson, C. N. Weiler, R. M. Camacho, P. T. Rakich, A. I. Young, M. J. Shaw, T. B. Pittman, J. D. Franson, and B.C. Jacobs, *Phys. Rev. A* **87**, 023808 (2013).
- [15] B. C. Jacobs and J. D. Franson, *Physical Review A* **79**, 063830 (2009).
- [16] J. D. Franson, B. C. Jacobs, and T. B. Pittman, *Physical Review A* **70**, 062302 (2004).
- [17] T. Gu, N. Petrone, J. F. McMillan, A. van der Zande, M. Yu, G.-Q. Lo, D.-L. Kwong, J. Hone, and C. W. Wong, *Nature Photonics* **6**, 554 (2012).
- [18] E. Hendry, P. J. Hale, J. Moger, A. K. Savchenko, and S. A. Mikhailov, *Physical Review Letters* **105**, 097401 (2010).
- [19] Q. Bao and K. P. Loh, *Nano Letters* **6**, 3677 (2012).
- [20] H. Yang, Hongzhi, X. Feng, Q. Wang, H. Huang, W. Chen, A. T. S. Wee, W. Ji, *Nano Letters* **11**, 2622 (2011).
- [21] E. A. Henriksen and J. P. Eisenstein, *Phys. Rev. B* **82**, 041412 (2010).
- [22] See, for example, *Graphene Nanoelectronics: Metrology, Synthesis, Properties and Applications* edited by H. Raza (Springer, Berlin Heidelberg New York, 2012).
- [23] J. Yan, M. H. Kim, J. A. Elle, A. B. Sushkov, G. S. Jenkins, H. M. Milchberg, M. S. Fuhrer, and H. D. Drew, *Nature Nanotechnology* **7**, 472 (2012).
- [24] E. J. Nicol and J. P. Carbotte, *Physical Review B* **77**, 155409 (2008).
- [25] E. McCann, *Physical Review B* **74**, 161403 (2006).
- [26] X. Wang, Y. P. Chen, and D. D. Nolte, *Optics Express* **16**, 22105 (2008).

- [27] The value of ϵ_r for BLG will vary somewhat according to the choice of substrate, which affects only the irradiance prefactor, $1/I^n$, in the n -photon absorption coefficient, β_n .
- [28] V. Nathan, A. H. Guenther, and S. S. Mitra, JOSA B **2**, 294 (1985).
- [29] D. C. Hutchings and E. W. Van Stryland, JOSA B **9**, 2065 (1992).
- [30] J. Rioux, G. Burkard, and J. E. Sipe, Physical Review B **83**, 195406 (2011).
- [31] For plots labeled $\Delta = 0$, we employed a gap value of $\Delta = 10^{-5}\gamma_1$ in the corresponding computations.